Journal of Metals, Materials and Minerals, 34(2), 1932, 2024

Leonardite humic acid activated carbon/MnO_2 composite nanostructures for supercapacitors

Artit AUSAVASUKHI[1], Thanchanok SIRIPHALA[2], Wanwisa LIMPHIRAT[3], and Sukanya NILMOUNG[2,*]

[1] *Department of Applied Chemistry, Faculty of Sciences and Liberal Arts, Rajamangala University of Technology Isan, Nakhon Ratchasima 30000, Thailand*

[2] *Department of Applied Physics, Faculty of Sciences and Liberal Arts, Rajamangala University of Technology Isan, Nakhon Ratchasima 30000, Thailand*

[3] *Synchrotron Light Research Institute (Public Organization), Nakhon Ratchasima, 30000, Thailand*

***Corresponding author e-mail**: sukanya.ni@rmuti.ac.th

Received date:
13 January 2024
Revised date
16 March 2024
Accepted date:
12 April 2024

Keywords:
Leonardite humic acid;
Activated carbon;
MnO_2;
Electrochemical properties;
Supercapacitors

Abstract

This work reports the preparation and electrochemical studies of activated carbon derived from leonardite humic acid composited with MnO_2 for supercapacitors. Activated carbon contains high conductivity, high specific surface area, and accommodates large volume expansion/contraction during charging/discharging process. Meanwhile, MnO_2 has very high theoretical specific capacity (1370 $F{\cdot}g^{-1}$). Their composite could significantly improve both the storage performance and cycle stability of supercapacitors. Moreover, humic acid from leonardite was selected to add value to this waste and reduce environmental pollution. By varying the carbonization temperature (500°C to 800°C), the prepared samples carbonized at 800°C exhibited fascinating properties. The oxidation state of Mn ions was in the mixed state of Mn^{+2} (41.2%) and $Mn^{+2,\,+3}$ (52.8%). A gravimetric capacitance of 329 $F{\cdot}g^{-1}$ and 294 $F{\cdot}g^{-1}$ were observed at 2 mVs^{-1} and 0.5 Ag^{-1}, respectively. The remaining gravimetric capacitance of 193 $F{\cdot}g^{-1}$ was evaluated at 1000 cycles, indicating its high cycle performance. Moreover, the gravimetric energy of 37.51 $Wh{\cdot}kg^{-1}$ and gravimetric power of 272.96 $W{\cdot}kg^{-1}$ were observed. When combined, the interesting electrochemical properties of leonardite humic acid-activated carbon/MnO_2 composite nanostructures make them important options for supercapacitor application.

1. Introduction

Supercapacitors are energy storage devices used in different fields, such as electronic equipment, data backup, hybrid electric vehicles, portable devices, and other fields [1]. These devices exhibit some unique features such as higher gravimetric power and longer cycle life than conventional capacitors [2]. Depending on the charge storage mechanism, supercapacitors are classified into two types: electric double-layer capacitors (EDLC) and pseudocapacitors. EDLCs store charge via the adsorption/desorption of electrolyte ions between the interface of electrode and electrolyte [3], while pseudocapacitors store energy through a redox process occurring near the surface of electrodes [4]. As it is well known, the electrochemical performance of energy storage devices is significantly influenced by the electrode materials. Therefore, improving the electrochemical properties of electrode materials is a great necessity. Activated carbon is one of the materials commonly used as an electrode material for EDLCs due to its high surface area and conductivity [5]. However, poor gravimetric capacitance and energy density are yet to be improved [6]. On the other hand, various metal oxides are commonly used as electrode materials for pseudocapacitors [7]. These pseudocapacitive materials produce larger gravimetric capacitance due to redox reactions [8]. Among them, manganese dioxide (MnO_2) is desirable due to its high theoretical gravimetric capacitance (1370 $F{\cdot}g^{-1}$), large potential range (0.9 V to 1.0 V), low chemical corrosion, natural abundance, and low toxicity [9-11]. MnO_2 crystals exist in several crystallographic forms, including α-MnO_2 (cryptomelane, JCPDS No. 44-0141), β-MnO_2 (pyrolusite, JCPDS No. 24-0735), γ-MnO_2 (nsutite, JCPDS No. 14-0644), and δ-MnO_2 (birnessite-type, JCPDS No. 80-1098). The α-MnO_2 structure is especially promising as a possible electrode material for energy storage devices [12,13]. However, poor electrical conductivity (10^{-8} $S{\cdot}cm^{-1}$), poor ion diffusion constant, large volume expansion, or poor structural stability of α-MnO restrict the achievement of high electrochemical activities in energy storage devices [14]. Mixing or coating MnO_2 with activated carbon is required to overcome these drawbacks. Activated carbon provides high conductivity and high specific surface area, whereas MnO_2 can store energy via redox reaction and shorten ion diffusion distance. The combination of these two materials could provide unique advantages in electrochemical performance. In recent years, various precursors for activated carbon have been used, including polyacrylonitrile, pitch, rayon, etc. However, with their high cost and environmental toxicity, new precursor materials from nature are gaining attention, including biowastes, agricultural wastes, etc. Leonardite is a byproduct of lignite mines and is predominately

made of carbon (55 wt%) [15]. It is well known that leonardite is a natural source of humic acid (HA), humin, and fulvic acids. Humic acid is one of the sources of activated carbon. This work focused on the synthesis of porous carbon from humic acid via the carbonization process. The advantage of using humic acid from leonardite as a source of activated carbon include its complex composition of molecules of highly functionalized carbon [16,17], a high specific surface area, is inexpensive, and is environmentally friendly.

Herin, the preparation of leonardite humic acid-activated carbon composite with manganese dioxide (HAaC/MnO_2) was reported. The leonardite was obtained from the Mae Moh lignite mine in Lampang province, Thailand. The prepared samples were analyzed by XRD, TGA, BET, FE-SEM, TEM, XPS, and XAS techniques. The electrochemical performances were measured via CV and GCD techniques. The results showed that HAaC/MnO_2 composite carbonized at 800°C had the highest gravimetric capacitance and cyclic stability.

2. Experimental

2.1 Materials

Leonardite was obtained from the Mae Moh lignite mine, in Thailand. Hydrochloric acid (37%, Mw 36.46 g·mol^{-1}, Qrec) and potassium hydroxide (>85%, Mw 56.1 g·mol^{-1}, Carlo Ebra) were used as the precursor substances for extracting humic acid from leonardite. Pluronic (12600 g·mol^{-1}: Sigma-Aldrich), manganese chloride (≥ 99%, Mw 197.91 g·mol^{-1}, Alfa Aesar), and ethanol (99.9 %, Mw 46.07 g·mol^{-1}, Qrec) were used for preparing manganese oxide. Nafion (5% w/w in water, 0.93 g·mL^{-1}, Alfa Aesar) was used to prepare the working electrode while the electrolyte solution used in this work was sulfuric acid (98%, Mw 98.08 g·mol^{-1}, ACI Labscan).

2.2 Synthesis of leonardite humic acid activated carbon/MnO_2 composite nanostructures

First of all, the Humic acid (HA) was extracted from leonardite by treating it with a potassium hydroxide solution (0.2 M). Then, the precipitated solid of Humic acid was treated with hydrochloric acid.Briefly, humic acid was prepared by refluxing 10 g of leonardite powder in 100 mL of potassium hydroxide solution at 80°C for 3 h. The soluble solution was centrifuged at 500 rpm for 15 min. The pH was adjusted to 2 by adding hydrochloric acid (36%) followed by centrifugation at 500 rpm for 15 min. The solid product was washed several times using distilled water and then dried at 90°C for 24 h to obtain pure humic acid. The humic acid-activated carbon (HAaC) from the leonardite composite with MnO_2 was prepared by the sol-gel method followed by the carbonization and physical activation process, respectively. Four grams of humic acid, 1 g of Pluronic powder, and 0.50 g molars of manganese (II) chloride were mixed into 20 mL of ethanol solvent. The solution was converted into a gel by stirring and heating it at 90°C overnight. After that, the gel materials were carbonized at various temperatures (500°C, 600°C, 700°C, 800°C) for 4 h under an argon atmosphere, followed by activated at 800°C for 2 h in a carbon dioxide atmosphere. In this process, CO_2 reacts with a carbon atom and removes some of the carbon atoms to generate porosity ($C + CO_2 \rightarrow 2CO$). The final products of leonardite humic acid-activated carbon/MnO_2 composite nanostructures were designated as HAaC/MnO_2_500°C, HAaC/MnO_2_600°C, HAaC/MnO_2_700°C, and HAaC/MnO_2_800°C for humic acid activated carbon/MnO_2 carbonized at 500°C, 600°C, 700°C, and 800°C, respectively. It is noteworthy that the carbonization temperature of 500°C to 800°C is higher than that of the decomposition temperature of Pluronic (400°C) [18] therefore the role of carbon derived from Pluronic powder could be ignored. A schematic diagram of preparation for HAaC/MnO_2 composite nanostructures is shown in Figure 1.

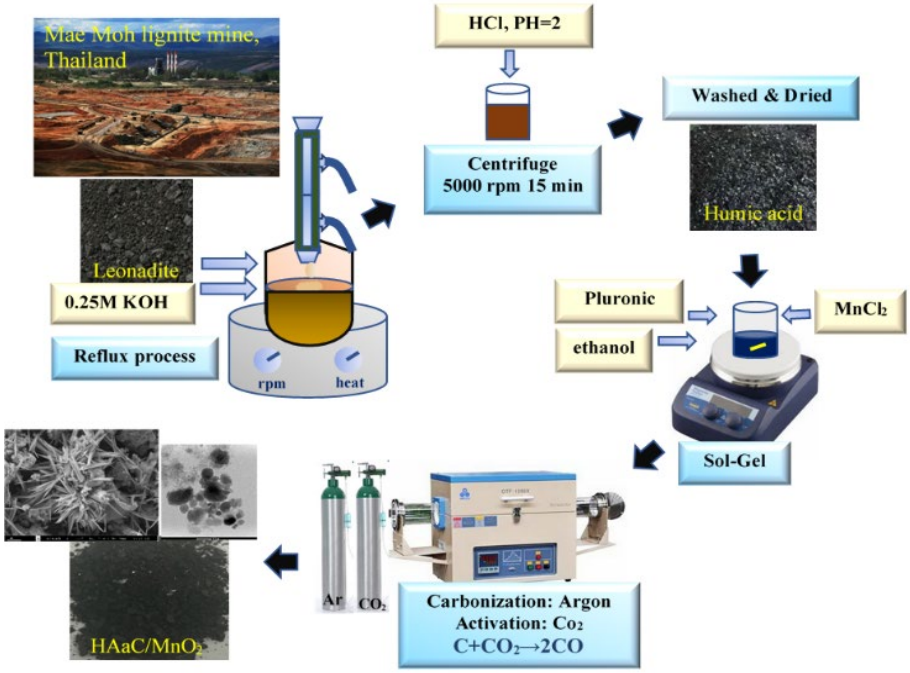

Figure 1. The schematic illustration of carbon/MnO_2 composite nanostructures preparation.

2.3 Materials characterization

The crystal structure study was performed by using powder X-ray diffraction (XRD, Rigaku). The morphologies were investigated using field emission scanning electron microscopy (FE-SEM, FEI). The microstructure was further investigated by transmission electron microscopy (TEM, FEI Tecnai G2). The thermal gravimetric analyzer (TGA, PerkinElmer) was used to estimate the content of activated carbon and MnO_2 in the prepared materials. The chemical compositions of metal atoms on the surface were conducted by XPS (XPS, KRATOS). To evaluate the oxidation state of manganese in MnO_2, X-ray absorption spectroscopy was performed at Beamline 8 (XAS, bending magnet, 1.2 GeV), SLRI, Thailand. Moreover, the specific surface area and porosity of materials were observed by the Brunauer-Emmett-Teller analyzer (BET, BEL SORP MINI II).

2.4 Electrochemical measurements

The electrochemical evaluation of the HAaC/MnO_2 prepared materials was tested via the auto lab station (PGSTAT 302N). A prepared active powder (5 mg), DI water (2 mL), methanol (0.4 mL), and 5 wt% Nafion (0.1 mL) were used to prepare the working electrode (WE). The slurry solution of 0.5 µL was dropped onto a glassy carbon electrode followed by drying with infrared for 10 min. In the measurement, a 1.0 M H_2SO_4 was used as the electrolyte solution. A platinum wire and an Ag/AgCl were used as the counter electrode (CE) and reference electrode (RE), respectively. The cyclic voltammogram was measured at various scan rates (2 $mV{\cdot}s^{-1}$ to 200 $mV{\cdot}s^{-1}$) within the potential range of –0.1 V to 1.0 V. The galvanostatic charge-discharge (GCD) spectra were obtained at current densities of 0.25, 1.0, 1.5, and 2.0 $A{\cdot}g^{-1}$. The data from electrochemical impedance spectroscopy (EIS) was evaluated in the frequency range of 5×10^5 to 0.1 Hz at the potential of 0.0 V.

3. Results and discussion

Figure 2 shows the XRD pattern of leonardite humic acid activated carbon/MnO_2 composite nanostructures carbonized at 500°C, 600°C, 700°C, and 800°C. The characteristic peaks of 16.91°, 24.79°, 28.49°, 36.41°, 37.28°, 40.65°, 50.79°, 59.60°, and 64.4° at 2θ were attributed to the reflections of (200) (220) (310) (400) (211) (301) (411) (521) and (002) crystal planes of α-MnO_2 (JCPDS No. 44-0141) [19]. It has been previously reported that the α-MnO_2 structure is a possible cathode for lithium-ion batteries [12,13]. The crystallinity percentage of MnO_2 was calculated by dividing the area of crystalline peaks by the area of all peaks, and multiplying the result by 100. The crystallinity percentages of 51.54, 45.63, 43.15, and 39.37 were observed for the samples carbonized at 500°C, 600°C, 700°C, and 800°C, respectively. Moreover, the crystallite size (D) of MnO_2 was calculated by the Scherrer equation. The values of 83 nm, 77 nm, 65 nm, and 58 nm were observed for the samples carbonized at 500°C, 600°C, 700°C, and 800°C, respectively. It was found that both the crystallinity percentage and the crystallite size decreased with an increase in the carbonization temperature. The diffraction peaks of carbon (JCPDS No. 75-1621) at about 26° and 42° could not be observed due to the amorphous state of carbon and the high crystallization degree of MnO_2 phases. Moreover, two asterisks indicated the impurity phases. It is assumed that the peaks at 27° and 32° correspond to the Quartz phase of Leonardite [20] and Humic acid (HA) peak [21], respectively.

Figure 3 shows SEM images of HAaCMnO$_2$ composite nanostructures carbonized at 500°C to 800°C, with a scale bar of 1 µm. The prepared samples exhibited nanowire characteristics within the carbon matrix. The average wire diameter of the samples carbonized at 500°C, 600°C, 700°C, and 800°C were 95.40 (SD = 30.00 nm), 122.54 (SD = 61.16 nm), 139.37 (SD = 64.67 nm), and 132.81 (SD = 45.85 nm) nm, respectively. It was expected that such nanoscale-prepared samples would improve the electrochemical performance of the electrode.

Figure 4(a) shows TEM bright field images of HAaC/MnO_2 composite nanostructures carbonized at 800°C. Two phases of HAaC and MnO_2 were observed. Figure 4(b) shows the selected area electron diffraction (SAED) profile of materials. The SAED pattern can be indexed to the (200) (310) (211) (411) (521) and (002) crystal planes of α-MnO_2 (JCPDS No. 44-0141), which was consistent with the XRD results. The spotty rings indicated a characteristic of nanocrystalline MnO_2. For the HAac area (Figure 4(c)), the absence of spotty rings indicates an amorphous characteristic of amorphous carbon materials.

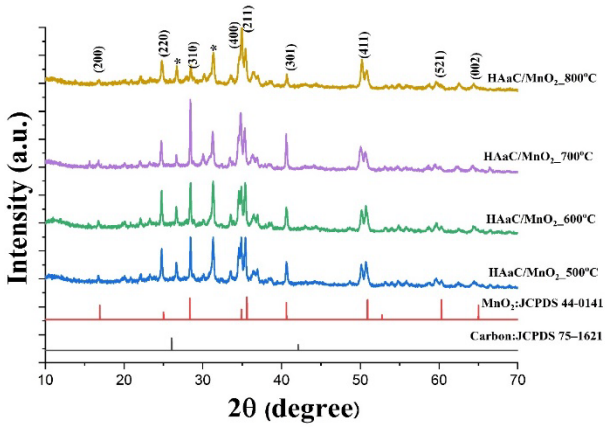

Figure 2. XRD patterns of HAaC/MnO_2 composite nanostructures at various carbonized temperatures.

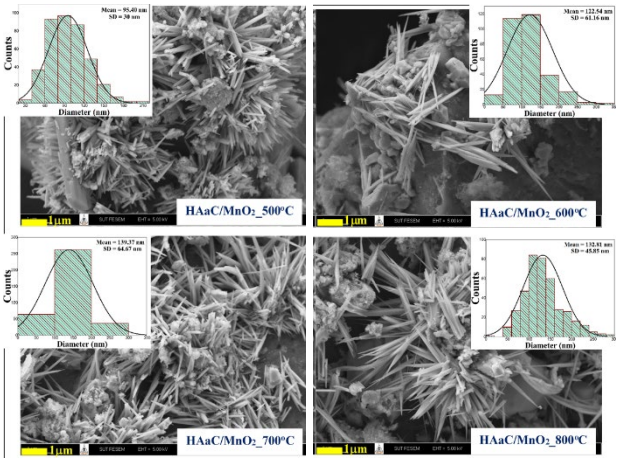

Figure 3. FE-SEM images of the HAaC/MnO_2 composite nanostructures carbonized at various carbonization temperatures

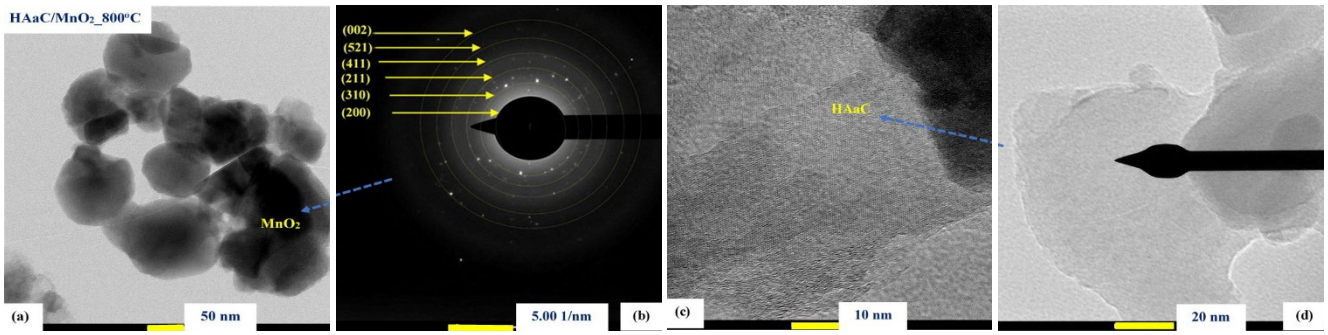

Figure 4. TEM images and corresponding SAED of the HAaC/MnO_2 composite nanostructures carbonized at 800°C.

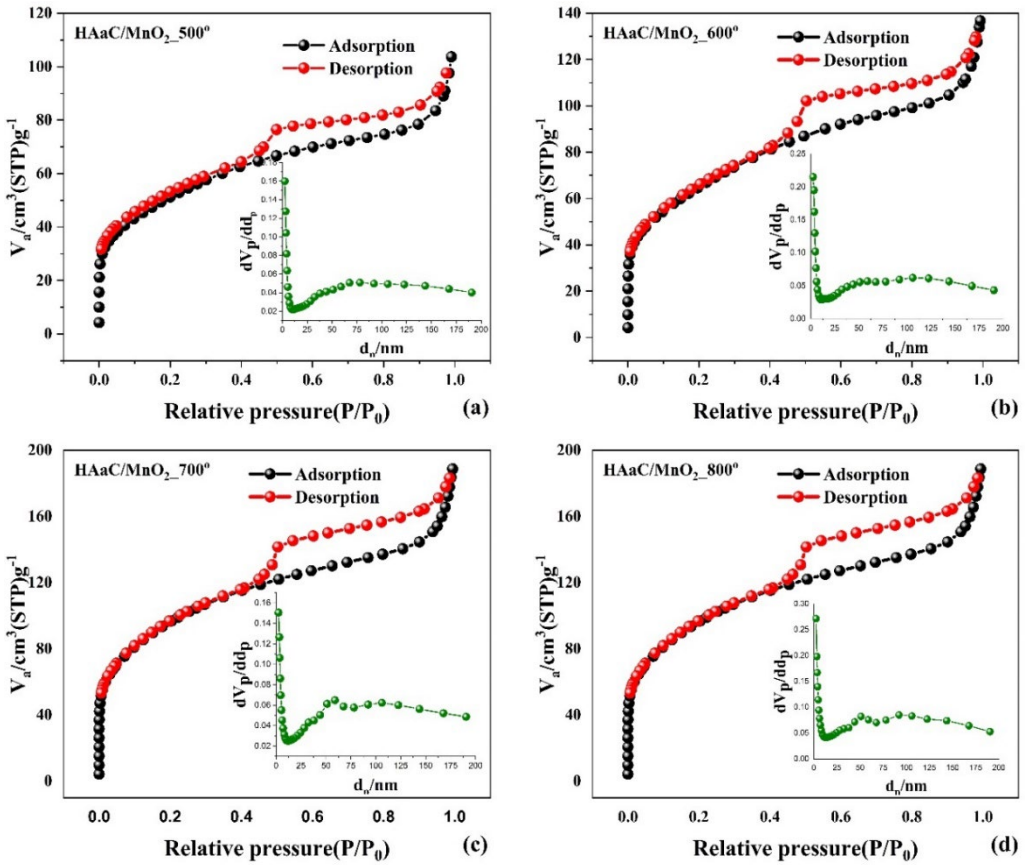

Figure 5. N_2 adsorption-desorption isotherm of the leonardite humic acid activated carbon/MnO_2 composite nanostructures.

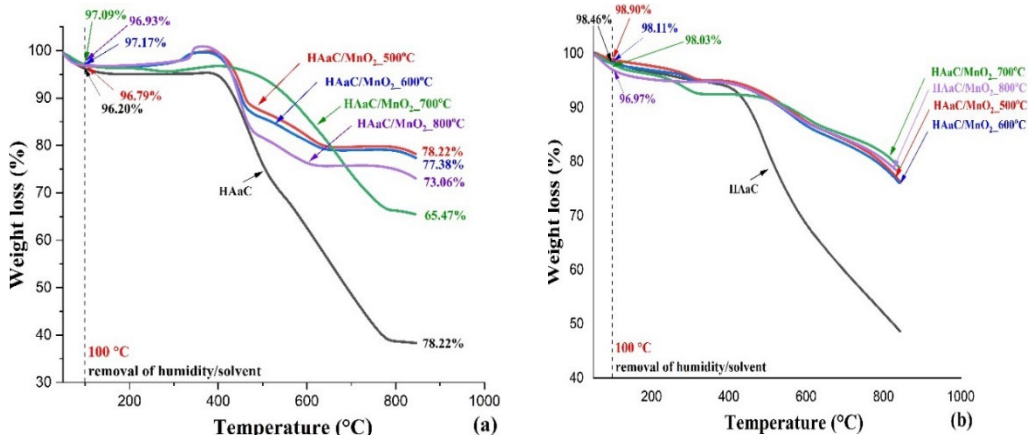

Figure 6. TGA spectra for HAaC/MnO_2 composite nanostructures under air (a), and argon (b) atmosphere.

Table. 1 specific surface area (a), pore volume (V), mean pore diameter (d_{mean}), weight percentage of the components, and the gravimetric capacitance (C_s) of HAaC/MnO_2 composite nanostructures carbonized at 500°C to 800°C.

HAac/MnO_2	A	V	d_{mean}	Weight percentage (%)			C_s ($F \cdot g^{-1}$)	
	($m^2 \cdot g^{-1}$)	($cm^3 \cdot g^{-1}$)	(nm)	MnO_2	Carbon	humidity	CV (2 $mV \cdot s^{-1}$)	GCD (0. 5 $A \cdot g^{-1}$)
500°C	180	0.1170	3.5483	78.22	18.57	3.21	210	153
600°C	231	0.1573	3.5839	77.38	19.79	2.83	258	221
700°C	169	0.1281	3.9211	65.47	31.62	2.91	213	141
800°C	337	0.1992	3.3745	73.06	23.87	3.07	329	294

Figure 5 shows the N_2 adsorption/desorption isotherm of the prepared samples. Type-IV (H4) isotherm was observed for all samples, indicating mesopores (2nm to 50 nm) [22]. Typically, the gravimetric capacitance of activated carbon strongly depends on the specific surface area [23,24]. It is well known that an electrode material with a large surface area provides high and rapid accessibility for electrolyte ions. Such behavior allows for high gravimetric capacitance [25]. Other parameters from the BET method are presented in Table 1. It was found that the prepared sample carbonized at 800°C showed a maximum specific surface area (337 $m^2 \cdot g^{-1}$) with the highest gravimetric capacitance (C_s).

Figure 6 shows the weight loss spectra for all prepared HAaC/MnO_2 composite nanostructures under air atmosphere (Figure 6(a)) and argon atmosphere (Figure 6(b)). The objective of testing the TGA under an argon atmosphere was to confirm the existence of carbon during the carbonization process. On the other hand, the heat treatment process under air atmosphere was to estimate the weight percentages of materials in the composite structure. Weight loss of pure HAaC was also tested for comparison. It was found that during measurements under air atmosphere, all samples exhibited three main steps of weight loss in the temperature range of ~50°C to 100°C ~400°C to 450°C, and ~450°C to 800°C, respectively. The slight weight loss (~3%) at temperatures below 100°C indicated the removal of solvent and humidity [26]. The dramatic weight loss between 400°C to 450°C and 450°C to 800°C was attributed to the oxidization of carbon components from Pluronic and humic acid, respectively [27]. After that, a short plateau was observed, indicating the complete decomposition of carbon components and the formation of crystalline MnO_2 as the metal decomposition product [28]. As known, EDLCs and pseudocapacitors are energy storage mechanisms associated with carbonaceous materials and metal oxides, respectively. Therefore, an appropriate proportion of residual content of activated carbon and MnO_2 may strongly support a high capacitance of the electrode. In this work, the weight percentage of MnO_2 loading in the HAaC/MnO_2 composite material was determined from residue weight loss at 850°C. The humidity was observed from the residue weight loss at 100°C, whereas the remaining weight was carbon. All results are presented in Table 1. Moreover, to confirm the existence of carbon at carbonized temperatures (500°C to 800°C), the thermal stability of the prepared composite materials was studied under an argon atmosphere (Figure 6(b)). It was found that the minor weight loss observed in the range of 50°C to 100°C, similar to those measured in air atmosphere, indicated the removal of absorbed humidity. As the temperature rose, an even weight loss was observed, which dramatically decreased at about 430°C. No plateau was observed until 850°C. Such behavior is assigned to the existence of carbon under carbonization temperature [29]. Interestingly, the percentage of carbon and MnO_2 for HAaC/MnO_2_600°C and HAaC/MnO_2_800°C were nearly similar. These two samples also exhibited higher gravimetric capacitance than others.

Figure 7 shows all electrochemical results for HAaC/MnO_2 composite nanostructures carbonized at 500°C to 800°C. Figure 7(a) shows the cyclic voltammogram at 0.2 $mV \cdot s^{-1}$ for all prepared electrodes. The rounded corners of the rectangular-like shape inferred the storage behavior of carbonaceous materials with resistances, while the peaks in the CV curves indicated a redox process arising from metal oxides [25]. The curve closure area of HAaC/MnO_2 carbonized at 800°C was much larger than the others, indicating its superior electrochemical performance. Two main peaks at about 0.45 V and 0.6 V corresponded to the anodic and cathodic peaks, respectively. The gravimetric capacitance (Cs) according to the CV curve was evaluated using the following equation:

$$C_s = \int I dV / m \upsilon \Delta V \quad (1)$$

Where the integral term is the area under the CV curve, m is the active mass in the prepared electrode, υ is the rate of scan (2 $mV \cdot s^{-1}$ to 200 $mV \cdot s^{-1}$), and ΔV is the potential range (–1.0 V to 1.0 V). Figure 7(b) shows that the gravimetric capacitance for all electrodes decreased with an increase in the scan rate. Such behavior was possibly due to less time for electrolyte ions to access the electrode materials at higher scan rates [30]. By varying the carbonization temperature, the sample carbonized at 800°C showed an excellent gravimetric capacitance value at 2 $mV \cdot s^{-1}$ (329 $F \cdot g^{-1}$) followed by 600°C (258 $F \cdot g^{-1}$), 700°C (213 $F \cdot g^{-1}$), and 500°C (210 $F \cdot g^{-1}$), respectively. According to the XRD analysis, the crystallinity percentage values of 51.54, 45.63, 43.15, and 39.37 were observed for the samples carbonized at 500, 600, 700, and 800°C, respectively. It was found that the specific capacitance did not directly depend on the crystallinity percentage of MnO_2. Two values did not follow the trend, particularly the samples carbonized at 600 and 700. However, both of them had nearly similar crystallinity values (45.63%, 43.15%). We assume that the electrochemical properties not only depended on the crystallinity of MnO_2 but also the synergistic effect between MnO_2 and carbon. The GCD technique was performed to confirm the results. Figure 7(c) displays GCD spectra at a current density of 0.5 $A \cdot g^{-1}$ for all prepared electrodes. The deviation of the GCD spectra from a straight line indicated the existence of redox reactions [31]. The gravimetric capacitance (C_s) from GCD spectra can be estimated using Equation (2):

$$C_s = I \Delta t / m \, \Delta V \quad (2)$$

where I is the constant discharge current, Δt is the discharge time, ΔV is the potential range (–1.0 V to 1.0 V), and m is the active mass

in an electrode. Among the GCD spectra, the discharge time of HAaC/MnO_2 carbonized at 800°C was longer than that of others. This electrode also showed the highest C_s values at all current densities (Figure 7(d)). The obtained results agreed well with the CV method. The corresponding specific energy and specific power are presented in Figure 7(e). The HAaC/MnO_2 carbonized at 800°C exhibited a maximum specific energy of 43 Wh·kg^{-1}. This value was slightly higher than those of 33.9 Wh·kg^{-1}for graphene/MnO_2 [32] and 34.56 Wh·kg^{-1} for porous carbon/MnO_2 [33].

To observe the stabilities of the HAaC/MnO_2_800°C electrode, the capacity retention at 1000 cycles was studied (Figure 8(a)). The capacities decreased from 329 F·g^{-1} (1st cycle) to 193 F·g^{-1} (1000th cycle). The decreasing value may be attributed to the damaged cell structure arising from the redox reaction. Moreover, the absence of redox peaks at the 1000th cycle indicated the influence of EDLCs in the charge/discharge mechanism. Besides the specific surface area, the specific conductivity is an important parameter supporting the electrochemical performance of material electrodes. In this work, the Nyquist plot from the EIS technique was used to speculate the electrical conductivity (Figure 8(b)). At high frequency, the solution resistance (R_s) was located at the intercept on the *Z'* axis.

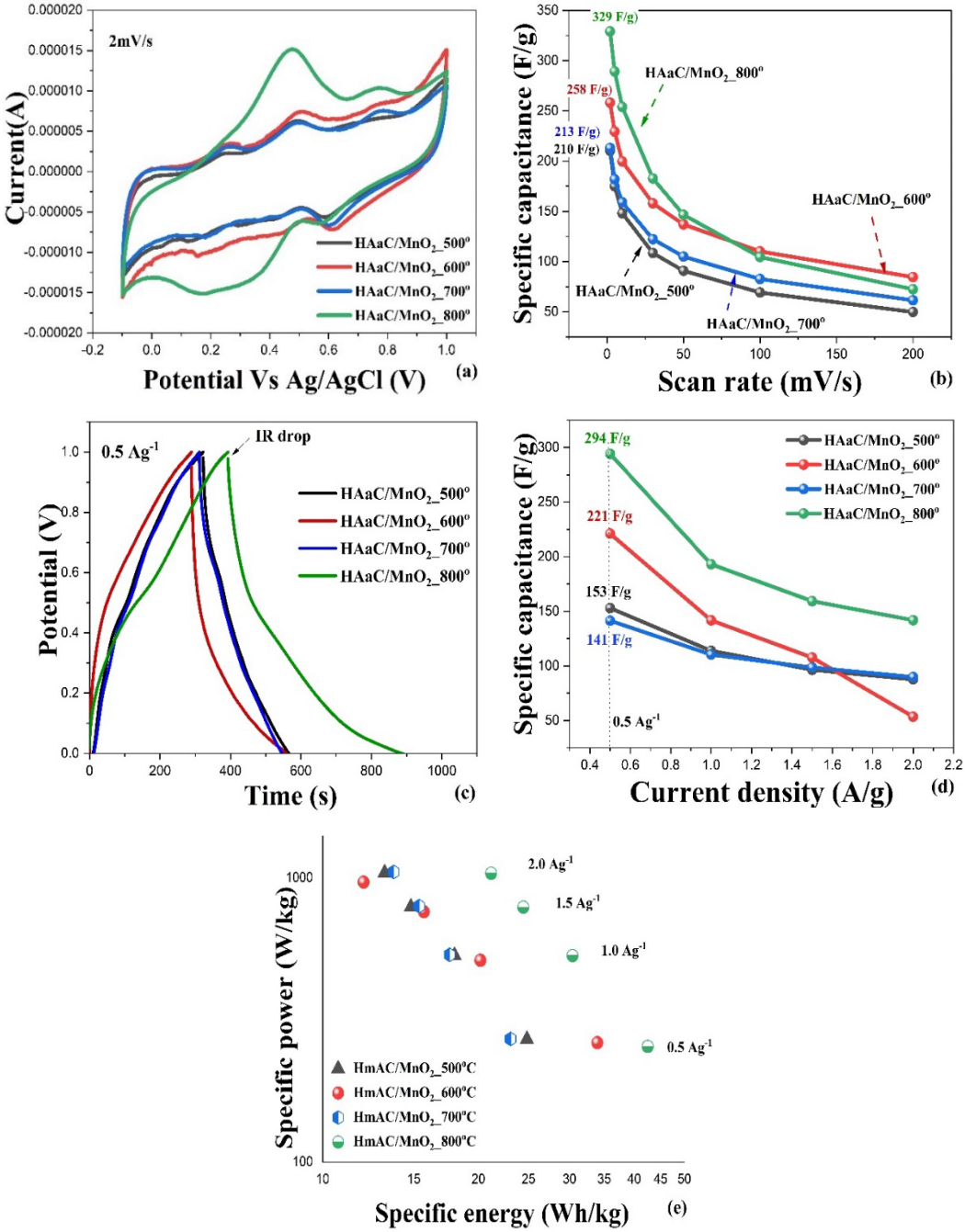

Figure 7. The cyclic voltammogram at 0.2 mV·s^{-1} (a); the gravimetric capacitance at various scan rates (2-200 mV·s^{-1}) (b); GCD spectra at 0.5 A·g^{-1} (c); variations of the gravimetric capacitance with current densities (0.5-2.0 A·g^{-1}) (d); and the specific energy against specific power of HAaC/MnO_2 electrodes (e).

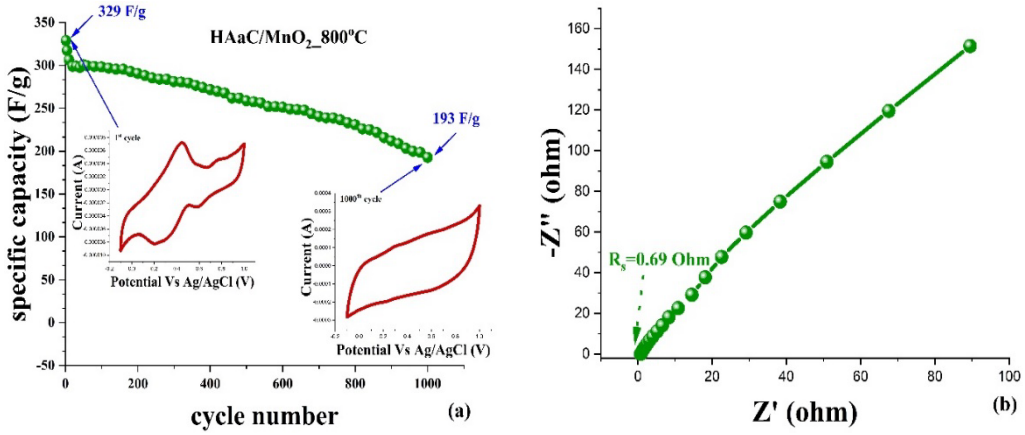

Figure 8. (a) The gravimetric capacity retention at 1000th cycle and (b) the Nyquist plot for HAaC/MnO_2_800°C.

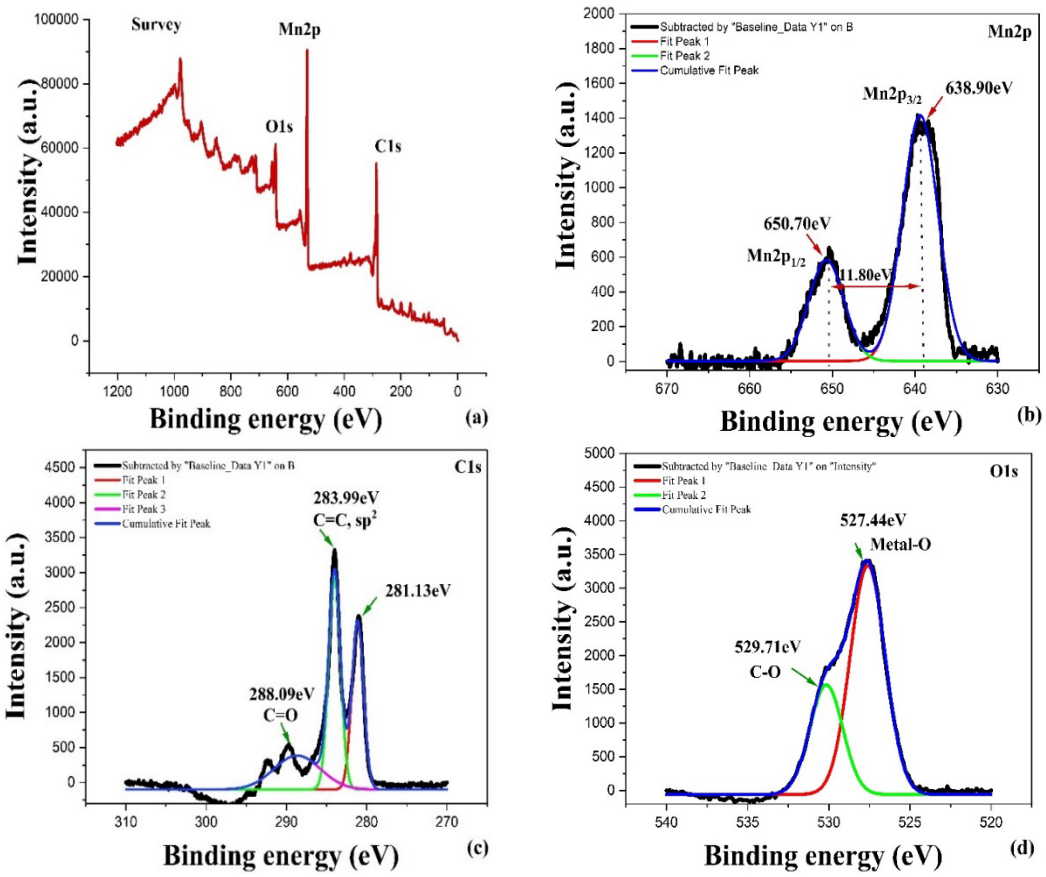

Figure 9. XPS spectra of Mn2p, C1s, and O1s for HAaC/MnO_2_800°C.

A low R_s value of 0.69 Ω was observed, indicating the large conductivity of materials. As expected, the high electrochemical properties of the HAaC/MnO_2_800°C electrode arose from: (i) the maximum surface area capable of supporting a large number of sites for accumulating electrolyte ions, (ii) high electrical conductivity and, (iii) the suitable content of carbon and MnO_2 in the composite material, resulting in the synergistic effect between the materials and to some extent, promoting the electrochemical performance. To get more details on the chemical compositions and the oxidation state of manganese ions in the HAaC/MnO_2_800°C structure, the XPS and XAS methods were employed.

Figure 9(a) shows the survey XPS spectra of the elements in the HAaC/MnO_2 composite nanostructures. The peaks at binding energies of 638.9 eV and 650.7 eV corresponded to Mn2p3/2 and Mn 2p1/2 binding energies, respectively, which were consistent with a previous report [34,35] (Figure 9(b)). A separation of 11.8 eV between these two peaks was observed. The peaks at 283.99 eV and 288.09 eV were attributed to lone pair bonding of carbon atoms to carbon (C=C) and oxygen (C=O), respectively (Figure 9(c)). The binding energies at 527.44 eV and 529.71 eV were related to the oxygen atom bonding with metal (O-Metal) and carbon atom (O-C), respectively (Figure 9(d)).

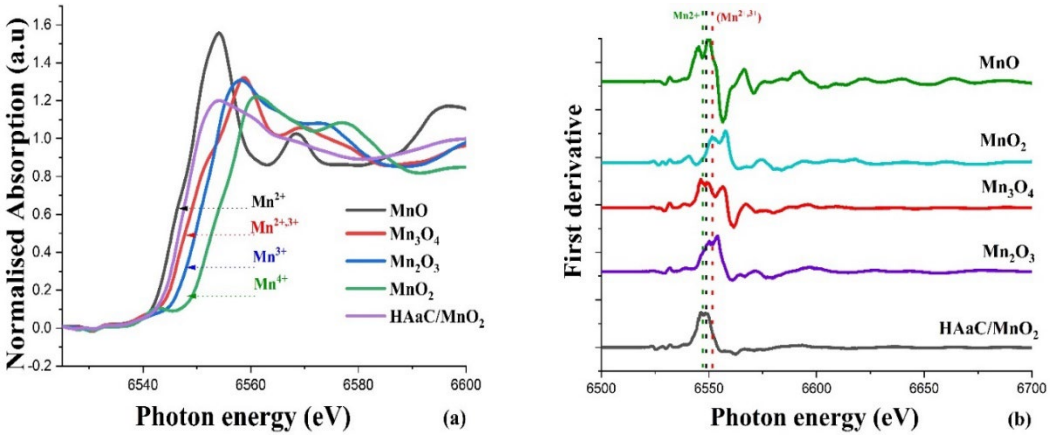

Figure 10. (a) Normalized XANEs spectra (b) the corresponding first derivative spectra, and (c) the linear combination fitting at Mn K-edge for HAaC/MnO_2_800°C.

Table 2. Linear combination fitting (LCF) data for HAaC/MnO_2_800°C.

Weight percentage			LCF-parameters	
MnO	Mn_3O_4	Chi-square	Reduced chi-square	R-factor
41.2	58.8	0.3017	0.00067	0.0045

Figure 10(a) shows the normalized EXAFS spectra at the manganese K-edge. The MnO, Mn_3O_4, Mn_2O_3, and MnO_2 were used as the references for the Mn^{2+}, $Mn^{2+,3+}$, Mn^{3+} and Mn^{4+}, respectively. The manganese edge energy of HAaC/MnO_2_800°C located between the profiles of MnO and Mn_3O_4 revealed that the Mn ions were in the mixed state of M^{2+} and $Mn^{2+,3+}$, which was further confirmed by the first derivative of EXAFS spectra (Figure 10(b)). It has been previously reported that the Mn^{2+}/Mn^{3+} exhibits high specific capacity and excellent 30000 cycle lifespans [36], while the Mn^{2+} effects on capacity fade in the lithium manganate-carbon system [37]. Excellent electrochemical properties of HAaC/MnO_2_800°C may arise from its mixed state. To observe the weight percentage of Mn^{2+} and $Mn^{2+,3+}$, the HAaC/MnO_2 spectra were fitted, and the results are listed in Table 2. A linear combination fitting showed that the HAaC/MnO_2 consists of 41.2% Mn^{2+} and 52.8% $Mn^{2+,3+}$.

4. Conclusions

Leonardite humic acid-activated carbon/ manganese dioxide composite nanostructures (HAaC/MnO_2) were prepared using a strategy that combined the sol-gel method with the heat treatment process. By varying the carbonization temperature (500°C to 800°C), all obtained samples exhibited nanowires with diameters less than 200 nm. The prepared samples carbonized at 800°C with mixed state of Mn^{+2} (41.2%) and $Mn^{+2,+3}$ (52.8%) showed excellent characteristics, i.e., a high specific surface area of 337 $m^2 \cdot g^{-1}$, low solution resistance (0.69 Ω), a high gravimetric capacitance of 329 $F \cdot g^{-1}$ (at 2 $mV \cdot s^{-1}$) and 294 $F \cdot g^{-1}$ (at 0.5 $A \cdot g^{-1}$), a gravimetric energy of 37.51 $Wh \cdot kg^{-1}$, and a gravimetric power of 272.96 $W \cdot kg^{-1}$. In addition, a gravimetric capacitance of 193 $F \cdot g^{-1}$ was observed at the 1000th cycle, indicating a high cyclic stability of the electrode. The high storage energy of this material can be attributed to its high electrical conductivity, maximum specific surface area, and high content of MnO_2.

Acknowledgments

This research was financially supported by the Energy Conservation and Promotion Fund [grant number 64-03-0028].

References

[1] D. Salinas-Torres, R. Ruiz-Rosas, E. Morallón, and D, Cazorla-Amorós, "Strategies to enhance the performance of electrochemical capacitors based on carbon materials," *Frontiers in Materials,* vol. 6, pp. 115, 2019.

[2] M. Shahedi Asl, R. Hadi, L. Salehghadimi, A. Goljanian Tabrizi, S. Farhoudian, A. Babapoor, M. Pahlevani, "Flexible all-solid-state supercapacitors with high capacitance, long cycle life, and wide operational potential window: recent progress and future perspectives," *Journal of Energy Storage,* vol. 50, pp. 104223, 2022.

[3] J. W. Long, D. B´elanger, T. Brousse, W. Sugimoto, M. B. Sassin, and O. Crosnier, "Asymmetric electrochemical capacitors stretching the limits of aqueous electrolytes," *MRS Bulletin*, vol. 36, pp. 513-522, 2011.

[4] Y. Huang, J. Liang, and Y. Chen, "An overview of the applications of graphene-based materials in supercapacitors," *Small,* vol. 8, pp. 1805-1834, 2012.

[5] A. Borenstein, O. Hanna, R. Attias, S. Luski, T. Brousse, and D. Aurbach, "Carbon-based composite materials for supercapacitor electrodes: A review," *Journal of Materials Chemistry,* vol 5, pp. 12653-12672, 2017.

[6] M. Liang, and H. Xin, "Microwave to terahertz: characterization of carbon-based nanomaterials," *IEEE Microwave Magazine,* vol. 15, pp. 40-51, 2015.

[7] S. Tajik, D. P. Dubal, P. Gomez-Romero, A. Yadegari, A. Rashidi, B. Nasernejad, Inamuddin, A. M. Asiri, "Nanostructured mixed

transition metal oxides for high performance asymmetric supercapacitors: facile synthetic strategy," *International Journal of Hydrogen Energy*, vol. 42, pp. 12384-12395, 2017.

[8] B. E. Conway. *Electrochemical Supercapacitor: Scientific Fundamentals and Technological Applications*. New York: Kluwer Academic/Plenum Publishers, 1999.

[9] S. Schrade, Z. Zhao, Z. Supiyeva, X. Chen, S. Dsoke, and Q. Abbas, "An asymmetric MnO_2 activated carbon supercapacitor with highly soluble choline nitrate-based aqueous electrolyte for sub-zero temperatures," *Electrochimica Acta,* vol. 425, pp. 140708, 2022.

[10] L. H. Tseng, C. H. Hsiao, D. D. Nguyen, P. Y Hsieh, C. Y. Lee, and N-H. Tai, "Activated carbon sandwiched manganese dioxide/graphene ternary composites for supercapacitor electrodes," *Electrochimica Acta,* vol. 266, pp. 218-292, 2018.

[11] Y. Xie, C. Yang, P. Chen, D. Yuan, and K. Guo, "MnO_2-decorated hierarchical porous carbon composites for high-performance asymmetric supercapacitors," *Journal of Power Sources,* vol. 425, pp. 1-9, 2019.

[12] S. Barbato, and J. L. Gautier, "Hollandite cathodes for lithium ion batteries: Thermodynamic and kinetics studies of lithium insertion into $BaMMn_7O_{16}$ (M=Mg, Mn, Fe, Ni)," *Electrochimica Acta,* vol. 46, no. 18, pp. 2767-2776, 2001.

[13] A. David, M. Tompsett, and S. Islam, "Electrochemistry of Hollandite α-MnO : Li-Ion and Na-Ion Incorporation," *Chemistry of Materials,* vol. 25, no. 12, pp. 2515-2526, 2013.

[14] J. G. Wang, F. Kang, and B. Wei," Engineering of MnO_2-based nanocomposites for high performance supercapacitors," *Progress in Materals Science,* vol. 74, pp. 51-124, 2015.

[15] R. P. Schwarzenbach, P. M. Gschwend, and D. M. Imboden, 1993. *Environmental organic Chemistry.* New Youk: John Wiley & Sons Inc.

[16] E. A. Ghabbour and G. Davies, *Humic Substances: Structures, Properties and Uses*. Cambridge: Special publication, 1998.

[17] S. Ozuzun, and B. Uzal, "Performance of leonardite humic acid as a novel superplasticizer in Portland cement systems," *Journal of Building. Engineering*, vol. 42, pp. 103070, 2021.

[18] B. A. G de Melo, F. L. Motta, and M. H. A. Santana, " Humic acids: Structural properties and multiple functionalities for novel technological developments," *Materials Science and Engineering C*, vol. 62, pp. 967-974, 2016.

[19] J. Luo, H. T. Zhu, H. M. Fan, J. K. Liang, H. L. Shi, G. H. Rao, J. B. Li, Z. M. Du, and Z. X. Shen, "Synthesis of single-crystal tetragonal α-MnO_2 nanotubes," *Journal of. Physical Chemistry C,* vol. 112, pp. 12594-12598, 2008.

[20] O. Canieren, C. Karaguzel, and A. Aydin, "Effect of physical pre-enrichment on humic substance recovery from leonardite," *Physicochemical. Problems of Mineral Processing*, vol. 53, no. 1, pp. 502-514, 2017.

[21] S. Sudiono, M. Yuniarti, D. Siswanta, and E. Kunarti, "The role of carboxyl and hydroxyl groups of humic acid in removing $AuCl_4$ from aqueous solution," *Indian Journal of Chemistry,* vol. 17, no.1, pp. 95, 2017.

[22] M. Králik, "Adsorption, chemisorption, and catalysis," *Chemical Papers*, vol. 68, no. 12, pp. 1625-1638, 2014.

[23] D. Wu, X. Xie, Y. Zhang, D. Zhang, W. Du, X. Zhang, and B. Wang, "MnO_2/carbon composites for supercapacitor: Synthesis and electrochemical performance," *Frontiers in Materials,* vol. 7, pp. 2, 2020.

[24] X. Wang, D. Wu, X. Song, W. Du, X. Zhao, and D. Zhang, "Review on carbon/polyaniline hybrids: design and synthesis for supercapacitor," *Molecules*, vol. 24, pp. 2263, 2019.

[25] S. Nilmoung, W. Limphirat, and S. Maensiri, "Electrochemical properties of ACNF/Li_2FeSiO_4 composite nanostructures for supercapacitors," *Journal of Alloys and Compounds*, vol. 907, pp. 164466, 2022.

[26] M. Fu, Z. Zhu, Z. Zhang, Q. Zhuang, F. Gao, W. Chen, H. Yu, and Q. Liu, "Microwave assisted growth of MnO_2 on biomass carbon for advanced supercapacitor electrode materials," *Journal of Materials Science*, vol. 56, pp. 6987-6996, 2021.

[27] S. Nilmoung, T. Sinprachim, I. Kotutha, P. Kidkhunthod, R. Yimnirun, S. Rujirawat, and S. Maensiri, "Electrospun carbon/$CuFe_2O_4$ composite nanofibers with improved electrochemical energy storage performance,"*Journal of Alloys and Compounds,* vol. 688, pp. 1131-1140, 2016.

[28] X. Wang, J. Chu, H. J. Yan, and H. K. Zhang, "Synthesis and characterization of MnO_2/Eggplant carbon composite for enhanced supercapacitors," *Heliyon,* vol. 82, pp. e10631, 2022.

[29] Y. Wang, Q. He, H. Qu, X. Zhang, J. Guo, J. Zhu, G. Zhao, H. A. Colorado, J. Yu, L. Sun, S. Bhana, M.A. Khan, X. Huang, D. P. Young, H. Wang, X. Wang, S. Wei, and Z. Guo, "Magnetic graphene oxide nanocomposites: Nanoparticles growth mechanism and property analysis," *Journal of Materials Chemistry C*, vol. 2, pp. 9478-9488, 2014.

[30] K. Wang, L. Huang, N. Eedugurala, S. Zhang, M. A. Sabuj, N. Rai, X. Gu, J. D. Azoulay, and T. N. Ng, "Wide potential window supercapacitors using open-shell donor–acceptor conjugated polymers with stable n-doped states," *Advanced Energy Materials*, vol. 9, pp. 1-8, 2019.

[31] X. Liu, L. Zhou, Y. Zhao, L. Bian, X. Feng, and Q. Pu, "Spherical nitrogen-rich porous carbon shells obtained from a porous organic framework for the supercapacitor," *ACS Applied Materials & Interfaces*, vol. 5, pp. 10280-10287, 2013.

[32] Y. Zhao, H. Hao, T. Song, X. Wang, C. Li, and W. Li, "MnO_2-graphene based composites for supercapacitors: Synthesis, performance and prospects" *Journal of Alloys and Compounds*, vol. 914, pp. 165343, 2022.

[33] Y. Xie, C. Yang, P. Chen, D. Yuan, and K. Guo, "MnO_2-decorated hierarchical porous carbon composites for high-performance asymmetric," *Journal of Power Sources*, vol. 425, pp. 1-9, 2019.

[34] Z. H. Huang, Y. Song, D. Y. Feng, Z. Sun, X. Sun, and X. X. Liu, "High mass loading MnO_2 with hierarchical nanostructures for supercapacitors," *ACS Nano*, vol. 12, pp. 3557-3567, 2018.

[35] H. Xu, X. Hu, H. Yang, Y. Sun, C. Hu, and Y. Huang, "Flexible asymmetric micro-supercapacitors based on Bi_2O_3 and MnO_2 nanoflowers: Larger areal mass promises higher energy density," *Advanced Energy Materials*, vol. 5, pp. 1401882, 2015.

[36] X. Li, Y. Tang, C. Han, Z. Wei, H. Fan, H. Lv, T. Cai, Y. Cui, W. Xing, Z. Yan, C. Zhi, and H. Li, "A static tin-manganese battery with 30000-cycle lifespan based on stabilized Mn^{3+}/ Mn^{2+} redox chemistry," *ACS Nano*, vol. 17, no. 5, pp. 5083-5094, 2023.

[37] C. Zhan, J. Lu, A. J. Kropf, T. Wu. A. N. Jansen, J. K. Sun, X. Qiu, and K. Amine, "Mn (II) deposition on anodes and its effects on capacity fade in spinel lithium manganate-carbon systems," *Nature Communications,* vol. 4, pp. 2437, 2013.